Stratification produced by surface cooling in lakes with significant shallow regions

Mathew Graeme Wells[1]

Research School of Earth Sciences, The Australian National University, Canberra, ACT 0200, Australia

Bradford Sherman

CSIRO Land and Water, GPO Box 1666, Canberra, ACT 2601, Australia

Abstract

A reservoir with distinct shallow and deep regions can produce stratification in response to uniform surface heat loss. The shallow region cools more rapidly, and a cold dense gravity current forms that results in stratification at the base of the deep region and an upwelling of cold water. The surface mixed layer deepens by convective entrainment, and a steady mixed-layer depth can result when the cold upwelling balances the rate at which the mixed layer deepens. The steady depth of the mixed layer depends on the ratio of the area of the shallow region to the area of the deep region. Significant stratification only results when the reservoir has shallow regions that account for more than 50% of the surface area. The depth of the surface mixed layer also depends on the ratio of the depths of the shallow and deep regions, and no significant stratification can form if this ratio is greater than 0.5. For a wedge-shaped geometry, these observations can be generalized by considering the ratio of the average depth to the maximum depth in a reservoir; the gravity current can produce stratification in more than 50% of the depth when this ratio is less than 0.5. Results from a laboratory study and field data from Chaffey Reservoir, Australia, are presented on the surface mixed-layer depth, along with estimates of the time scales needed for atmospheric forcing to lead to the development of stratification.

In many lakes, reservoirs, and estuaries, the interaction of surface cooling with sloping bathymetry results in the generation of gravity currents. For a given heat flux out of the water surface, the temperature of the water column decreases more rapidly in the shallow regions where the water column has less thermal mass than in the deep regions. This, in turn, produces a horizontal temperature (i.e., density) gradient that drives along the bottom a cold gravity current that transports cold, dense water as well as contaminants from the shallow to the deep regions. These downslope flows also can lead to the formation of stratification, even during winter when penetrative convection is often assumed to cause complete overturning of the water column. If the rate at which cold, dense water upwells, due to continued input by the cold gravity current, balances the rate at which the mixed layer deepens due to entrainment by surface convection, then a steady mixed-layer depth should result.

The formation of gravity currents has been observed in field studies by Monismith et al. (1990), where differential cooling due to variations in reservoir bathymetry or surface wind speed led to strong horizontal circulation in a reservoir. Gravity currents have been observed flowing down topography in Lake Geneva (Fer et al. 2000) and in Lake Tahoe (Thompson and Schladow pers. comm.) where they are believed to have filled the deep basin with dense, cold water. James and Barko (1991) observed gravity currents transporting significant amounts of phosphorus from the shallow to the deeper regions of Eau Galle reservoir. Thermistor chain data show the ubiquitous presence of convectively driven circulation in billabongs (Sherman et al. unpubl. data), shallow lakes, and wetlands (Arnold and Oldham 1997). The relationship between the volume flux of a gravity current, the surface cooling rates, and the sidearm geometry has been studied in the laboratory by Maxworthy (1997), Sturman and Ivey (1998), Sturman et al. (1999), and Finnigan and Ivey (1999, 2000) and numerically by Horsch and Stefan (1988).

Away from shallow regions, surface cooling of a reservoir leads to a well-mixed surface layer that can erode the deep, cold, stratified layer produced by the gravity current. In a laboratory study, Wells et al. (1999) investigated the competition between stratification and mixing from the combined presence of a buoyant plume and a distributed buoyancy source in a confined rectangular environment. By itself, the buoyant plume (analogous to the cold gravity current) caused the environment to stratify by filling the tank with dense fluid (Baines and Turner 1969). In contrast, the distributed buoyancy source made the entire water column overturn. When these two opposing processes were simultaneously present, a stratified lower layer and a convectively mixed upper layer developed. The depth of the convective region was found to depend on the ratio of the distributed : plume buoyancy fluxes. The interface retained a constant position with time while the density of both layers continued to increase at the same rate, resulting in a constant density step between the layers. The presence of the fixed density interface required also a balance between the volume flux due to mixed-layer deepening and the volume flux supplied by the plume.

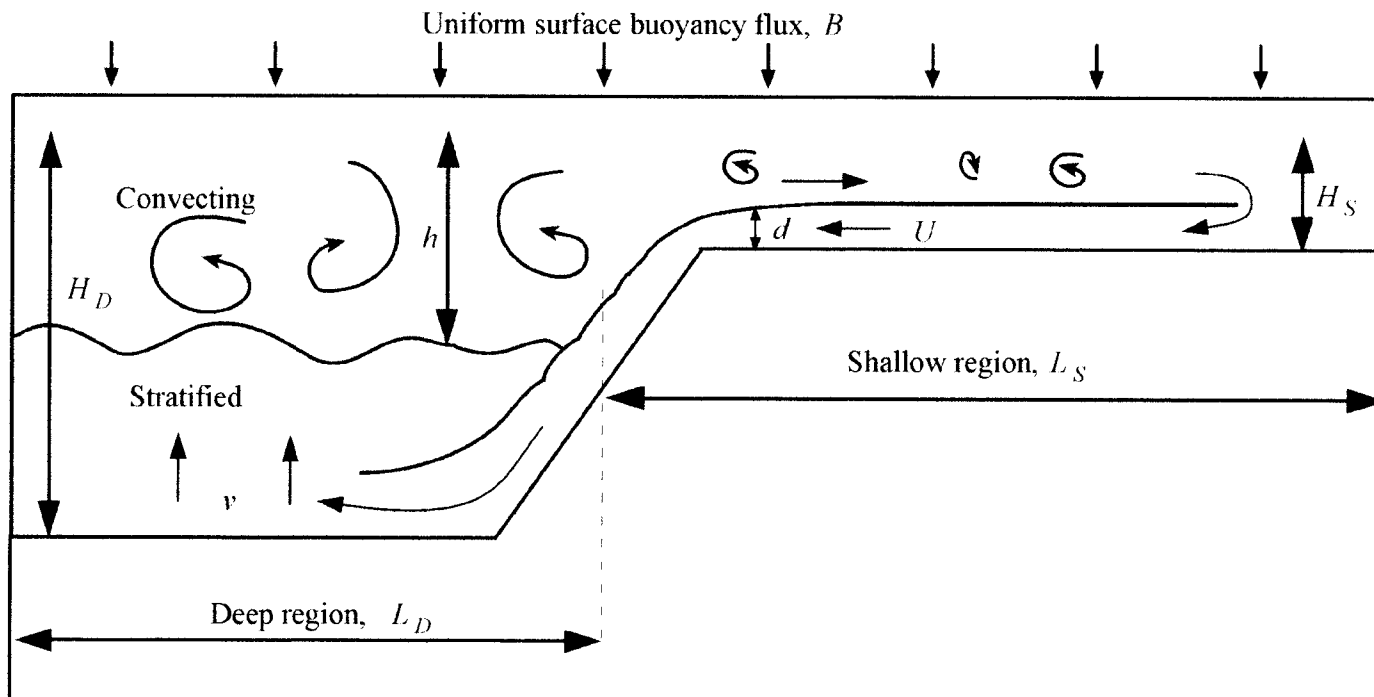In the present study, we describe field and laboratory ob-

Fig. 1. A uniform destabilizing buoyancy flux B is provided to the surface of a reservoir with a deep region of length L_D and depth H_D, which has a shallow side arm of length L_S and depth H_S. The shallow region cools rapidly and produces a gravity current of velocity U and initial thickness d. The gravity current fills the deep region with cold, dense fluid and causes a general upwelling with velocity v. Near the surface of the deep region, there is a convecting layer of depth h.

servations of how stratification can form due to prolonged surface cooling when a large area of a reservoir is relatively shallow. We consider the circulation and stratification of a simple reservoir with the bathymetry shown in Fig. 1, in which a uniform surface heat flux, $\tilde{H}$, drives the negative surface buoyancy flux, $B = g\alpha\tilde{H}/\rho C_p$. Negative fluxes represent heat lost from the water to the atmosphere. We show that the same type of stratification described by Wells et al. (1999) can occur when cooling of shallow side arms in a reservoir leads to a dense gravity current, analogous to the buoyant plume. We start by reviewing previous experimental studies of dense gravity currents that form by cooling a shallow side arm of a reservoir. Time scales for these gravity currents to fill a deep basin and stratify are then discussed. By considering the input of buoyancy into control volumes for the deep stratified layer and surface convective layer, we then derive a predicted equilibrium mixed-layer depth. Some restrictions on the stability of this layer are then discussed, and the predicted mixed-layer thickness is compared with a laboratory experiment and with field observations of winter stratification in a medium-sized reservoir. Conclusions are then presented on the application of this theory to predicting the existence of winter stratification based on reservoir bathymetry and surface cooling.

Theoretical background

Convective circulation time scales—Cooling on the shallow side arm of a reservoir surface results in horizontal density gradients that drive the formation of a dense, cold grav-

ity current. In laboratory studies of such cooling, Sturman and Ivey (1998) found that there was an initial period of disorganized overturning convection before horizontal density gradients started to drive a dense gravity current. This time scale, $\tau_{initial}$, was found by Finnigan and Ivey (1999) to depend on the length of the shallow region, L_s, the buoyancy flux, B, and the ratio of the thickness of the gravity current, d, to the depth of the shallow region, H_s, as

$$\tau_{initial} \sim L_s^{2/3}B^{-1/3}(1 - d/H_s)^{-1}$$

Experimental observations of d/H_s by Finnigan and Ivey (1999) and Grimm and Maxworthy (1999) found values in the range 0.25–0.33. This suggests that exchange occurs at a rate less than the theoretical maximum predicted by Armi (1986) to occur at $d/H_s = 0.36$.

The steady volume flux per unit width of the gravity current was found by Sturman and Ivey (1998) to vary as

$$\frac{Q}{W_S} = 0.2(BL_S)^{1/3}H_S \tag{2}$$

Experiments of Finnigan and Ivey (1999) and Grimm and Maxworthy (1999) found similar expressions for the volume flux, but with slightly different experimental constants. The time scale for the gravity current to fill the whole of the deep region of volume $V_D = W_D L_D H_D$ then becomes

$$\tau_{flush} \sim \frac{V_D}{Q} = 5L_D B^{-1/3}L_S^{-1/3}\frac{H_D}{H_S} \tag{3}$$

The steady circulation sketched in Fig. 1 can only become

Table 1. Nomenclature.

Symbol	Description	Units
g'	Normalized density anomaly $(g\Delta\rho/\rho)$	m s^{-2}
ρ	Density	kg m^{-3}
$\tilde{H}$	Heat flux	W m^{-2}
B	Buoyancy flux	m^2 s^{-3}
L_S, L_D, W_S, W_D	Lengths and widths of shallow and deep regions	m
A_S, A_D	Areas of shallow and deep regions	m^2
H_S, H_D	Depths of shallow and deep regions	m
h	Thickness of convective region	m
ζ	Normalized convective layer thickness ($=h/H_D$)	Dimensionless
R	Ratio of deep to shallow areas ($=A_D/A_S$)	Dimensionless
P	Ratio of shallow to deep depths ($=H_S/H_D$)	Dimensionless
d	Thickness of gravity current	m
$\tau_{initial}$	Flushing time scale for shelf region	s
τ_{flush}	Flushing time scale for deep region	s
Q	Volume flux of gravity current	m^3 s^{-1}
U	Velocity of gravity current	m s^{-1}
v	Vertical upwelling velocity	m s^{-1}
V	Reservoir volume	m^3
g	Gravitational constant	m s^{-2}
C_p	Heat capacity of water	J kg^{-1} C^{-1}
α	Coefficient of thermal expansion	C^{-1}

established if the duration of surface forcing is longer than both τ_{flush} and $\tau_{initial}$. If the surface forcing does not satisfy this criterion, then a deeper mixed layer would be expected because the gravity current either hasn't developed fully or cannot fill the deep region before the forcing finishes.

Steady convective layer depth—We consider control volumes for the surface mixed layer of constant depth h and a deep stratified layer of thickness $(H_D - h)$. Both layers have the same area $A_D = L_D W_D$. The discharge of the gravity current, $Q = Ud$, provides a buoyancy flux from the shallow to deep region that is exactly balanced by a surface return flow from the deep to the shallow region.

If the convective layer depth, h, is to remain constant, then the rate at which the gravity current forces the interface to upwell, v, must balance the rate at which penetrative convection causes the surface layer to deepen, dh/dt, against the imposed density gradient due to the gravity current. This requires that the density difference between the two layers remains constant (i.e., the densities of both layers change at the same rate).

Manins and Turner (1977) found that when a destabilizing buoyancy flux was applied to a linear density gradient, the depth of the convectively deepening mixed layer increased with time as

$$h = (6\eta B(N)^{-2}t)^{1/2} \tag{4}$$

where $N = -[(g/\rho)(d\rho/dz)]^{1/2}$ is the buoyancy frequency. The mixing efficiency, η, varies in theory from ⅓ for weak convection in systems with continuous density gradients to 1 in vigorously convecting systems with sharp density interfaces. In practice, the maximum value of η is 0.46 when interface entrainment is significant (Wells et al. 1999). Differentiating Eq. 4 and eliminating time gives the rate at which the convecting layer deepens,

$$\frac{dh}{dt} = \frac{3\eta B}{N(z)^2 h} \tag{5}$$

The rate at which the densities of both mixed and stratified layers increase must equal the rate of density increase of the entire system. This is due solely to the surface buoyancy flux applied across the total surface area, A, as

$$\frac{d\rho}{dt} = \frac{A\rho_0 B}{gV} \tag{6}$$

where g is the gravitational acceleration, V is the total reservoir volume, and ρ_0 is a reference density. For the particular geometry sketched in Fig. 1, Eq. 6 can be expressed as

$$\frac{d\rho}{dt} = \frac{(A_D + A_S)\rho_0 B}{g(A_D H_D + A_S H_S)} \tag{7}$$

Within the stratified layer $d\rho/dt$ must balance the induced upwelling velocity, v, of the density gradient. Thus, at every depth within the stratified region, the following relationship is satisfied,

$$\frac{d\rho}{dt} = -v\frac{d\rho}{dz} \tag{8}$$

The gravity current will generate a smooth density gradient in the deep region, but theory (Baines and Turner 1969) and experiments (Turner 1998) have shown that this gradient is not linear. The strongest stratification occurs at the interface between the mixed and stratified layers, and weaker stratification occurs at the depth the gravity current spreads out. This implies that for a constant rate of density change the upwelling velocity has a maximum at depth and is weaker at the interface. The divergence in the upwelling velocity is due to entrainment of fluid into the gravity current as it travels down along the slope.

Using Eqs. 7 and 8, the upwelling velocity is equivalent to

$$v(z) = \frac{B(A_D + A_S)}{N(z)^2(A_D H_D + A_S H_S)} \tag{9}$$

Equating the rate at which the interface deepens (Eq. 5) with the upwelling velocity of the density gradient at depth h (Eq. 9) gives

$$\zeta \equiv \frac{h}{H_D} = 3\eta\frac{R + P}{R + 1} \tag{10}$$

where $\zeta = h/H_D$ is the normalized mixed-layer depth, $P = H_S/H_D$ is the ratio of the depths of the shallow and deep regions, and R is the ratio of the deep and shallow areas,
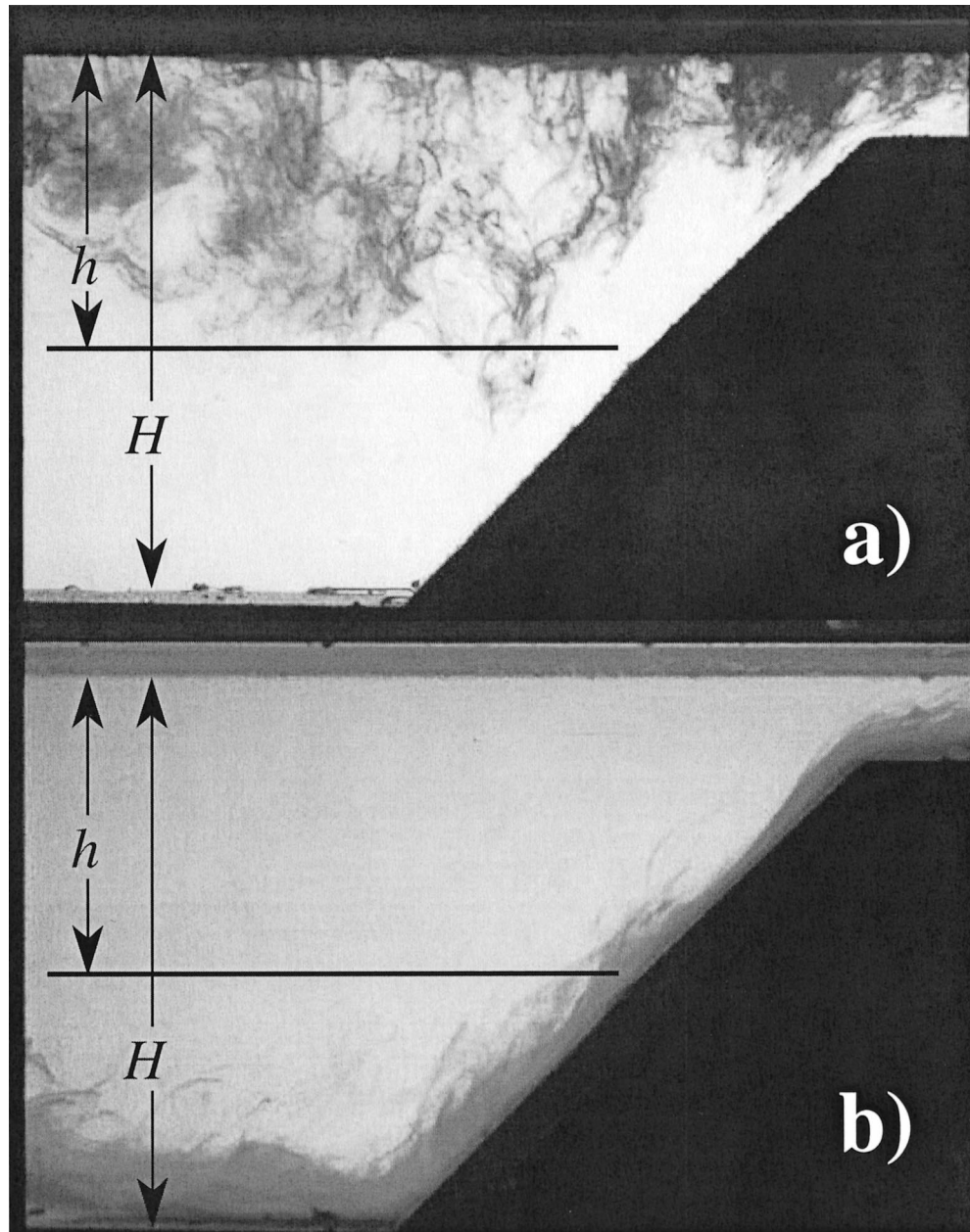
Fig. 2.   Photographs showing the circulation of dye in the experiment for $R = 0.5$. The dye is placed into the convecting layer of depth h (a) or in the gravity current (b).

$$R = \frac{A_D}{A_S} = \frac{L_D W_D}{L_S W_S} \qquad (11)$$

The mixed layer penetrates to full depth ($\zeta = 1$) as R becomes very large. When $P = 0$, the normalized mixed-layer depth, ζ, is essentially the same as that given by Wells et al. (1999) for the case of a point source plume.

A more general interpretation of Eq. 10 in terms of the bathymetry of a reservoir was made by an anonymous reviewer. The mean depth, H_{mean}, of the reservoir is simply the ratio of the total volume to the total area of the reservoir so that Eq. 6 can be replaced by

$$\frac{d\rho}{dt} = \frac{\rho_0 B}{g H_{mean}} \qquad (12)$$

Using Eqs. 5, 8, and 12, the steady mixed-layer depth can be expressed as

$$\zeta = 3\eta \frac{H_{mean}}{H_{max}} \qquad (13)$$

For the geometry in Fig. 1, $H_{mean}/H_{max} = (R + P)/(R + 1)$ so that Eq. 13 is equivalent to Eq. 10. The generality of Eq. 13 can be found by considering geometries that often occur in the field, such as a triangular wedge where $H_{mean}/$
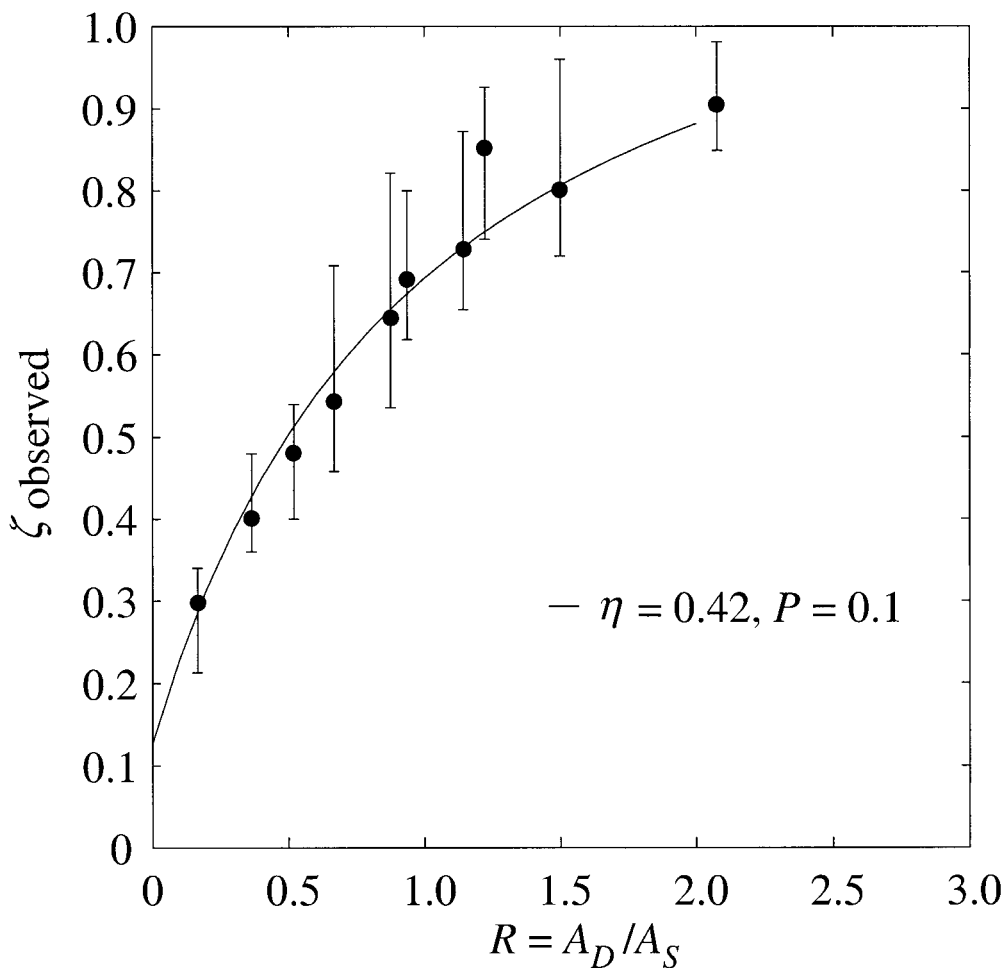
Fig. 3. Experimental results of the normalized convecting layer depth ζ as a function of R, the ratio of deep to shallow areas. The theoretical result of Eq. 10 is shown for $P = 0.1$ and agrees well with data.

$H_{max} = \frac{1}{2}$ and $\zeta = \frac{2}{3}\eta$; and a conical basin where $H_{mean}/H_{max} = \frac{1}{3}$ and $\zeta = \eta$. In the limit of a rectangular tank, $H_{mean}/H_{max} = 1$ so that $\zeta = 3\eta$, implying that mixing will eventually occur to full depth, as expected. If a reservoir's bathymetry is known, the value of the mixed-layer depth can easily be calculated using Eq. 13. The application and limits of this interpretation will be discussed in terms of our experimental and field results.

Laboratory experiments

Methods—Laboratory experiments were performed in a rectangular tank 1.2 m long × 0.2 m wide × 0.4 m deep with geometry as shown in Fig. 1. The base was made of copper, and sidewalls were insulated with 15 mm of polystyrene foam. Rather than provide cooling from the upper surface, we found it easier to invert the setup and heat from the base using two electric heat pads that allowed the deep and shallow regions to be heated independently. Before each experiment, the tank was filled with fresh water at the laboratory temperature. The heat flux was then started over the base of the whole tank. The buoyancy flux was the same in all experiments and had a value of 10^{-5} m² s⁻³.

The ratio, R, was varied by changing the relative length of the deep and shallow regions. In initial experiments, the deep regions had $H_D = 280$ mm and a shallow depth of $H_S = 40$ mm. Later experiments systematically varied the ratio $P = H_S/H_D$.

To determine the flushing time scale of the deep region (Eq. 3), we conducted one experiment with $R = 1$ and $P = \frac{1}{5}$, where only the shallow region was heated. A gravity current formed that stratified the whole of the deep region after 12 min, in agreement with Eq. 3. All experiments were run for at least twice this time to ensure a steady balance in the convective depth.

Development of the circulation: Immediately after the initiation of heating, thermals formed in the deep region that initially mixed the whole depth of the water column. After 3–5 min, large horizontal temperature differences were set up between the deep and shallow areas, and a gravity current
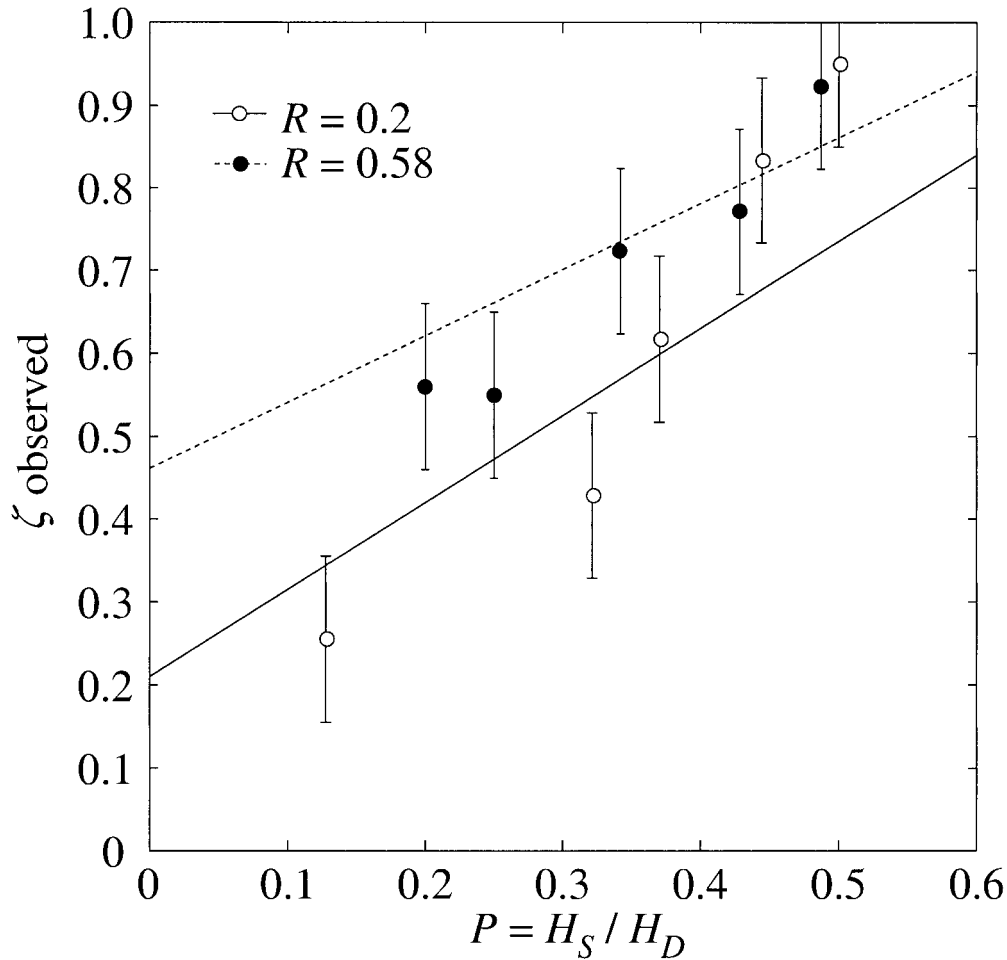
Fig. 4. Experimental measurements of the normalized convecting layer depth ζ as a function of the ratio of shallow to deep depths, $P = H_S/H_D$, for a given area ratio R. The theoretical result of Eq. 10 is shown for $R = 0.2$ and $R = 0.58$.

started to stratify the deep region. The time scale for the initiation of the gravity current was consistent with Eq. 1. After approximately 12 min, the thermals in the deep region were influenced by the stratification and no longer penetrated the full depth of the deep region; by about 15 min, the up-welling of the deep region had forced the interface depth to the steady depth given by Eq. 10.

In some experiments, heating was commenced in the shallow region 20 min before it commenced in the deep region in order to establish a strong stratification. The surface convection subsequently eroded the stratification within 15 min, and the same steady state was attained as in the other experiments. Similarly, when the heating was turned off so that the circulation stopped, the circulation was reestablished 5 min after the heating restarted, consistent with Eq. 1.

To visualize the circulation in the experiments, food dye was added to the water in the shallow and deep regions. Photographs of the circulation are shown in Fig. 2, where we have inverted the images so that they appear to be cooled from the surface as in Fig. 1. The well-mixed surface layer can be seen in Fig. 2a, where dye is transported by thermals to an average depth h, marked by a horizontal line. The

dense gravity current can be seen in Fig. 2b, where dye had been added to the shallow region. This dye was subsequently observed to fill the deep region, and further input of dense fluid by the gravity current advected the dye into the well-mixed surface layer.

Results—Two sets of experiments were conducted. The first tested the dependence of the surface mixed-layer depth on the relative surface areas of shallow and deep regions, as described by Eq. 10. The thickness of the convecting region was estimated visually by injecting dye into the layer, as shown in Fig. 2a. In these experiments, the shallow depth was, at most, $\frac{1}{5}$ of the deep layer depth (i.e., $P = H_S/H_D \le$ 0.2. Agreement with theory is good (Fig. 3), and we see that for $R > 2$ the entire depth is essentially well mixed.

The size of the error bars reflects the thickness of the interface. Experimental studies (Deardorf et al. 1980) found that even for very stable interfaces the normalized interface thickness $\Delta h/h$ had a significant magnitude and that the thickness of the interface is a function of a Richardson number, Ri_g. For $5 < Ri_g < 40$, their empirical relationship is
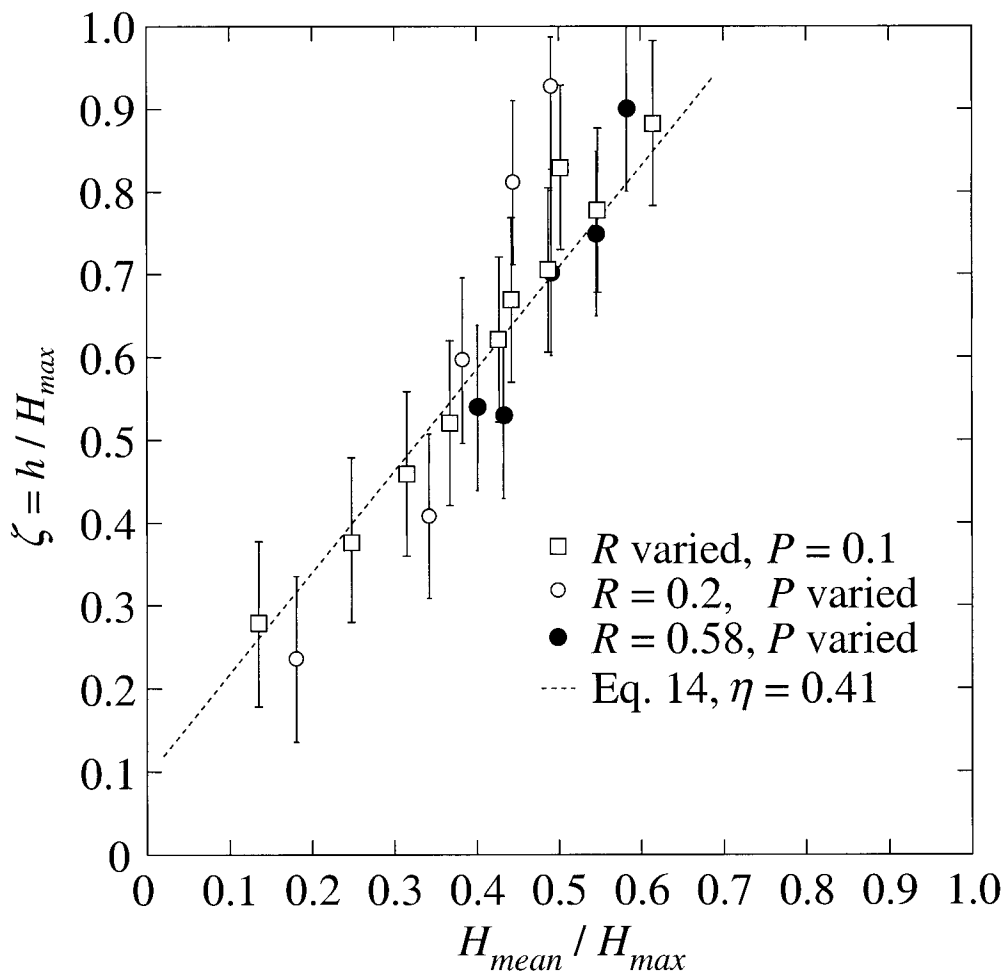
Fig. 5. Experimental results of the normalized convecting depth, ζ, as a function of the ratio of the mean depth to the maximum depth of the tank. The theoretical result of Eq. 13 is shown as a dashed line. The data are the same as plotted in Figs. 3, 4.

$$\frac{\Delta h}{h} = 0.21 + 1.31 \mathrm{Ri}_g^{-1} \qquad (14)$$

The Richardson number, Ri_g, is given by

$$\mathrm{Ri}_g = \frac{g'h}{w^{*2}} \qquad (15)$$

where $g' = \Delta\rho/\rho$ is the normalized density anomaly of the interface density step $\Delta\rho$ and w^* is the root mean square eddy velocity of the convective motions descending from the surface to a depth h. Experimental and theoretical work of Adrian et al. (1986) has determined that w^* is described by

$$w^* = 0.6(Bh)^{1/3} \qquad (16)$$

The second set of experiments looked at the dependence of the normalized mixed-layer depth, ζ, on the depth ratio $P = H_S/H_D$ for a given area ratio R (Eq. 11). Experimental results are shown in Fig. 4, and ζ can be seen to increase with P. Theoretical values of ζ given by Eq. 10 are plotted for $R = 0.2$ and $R = 0.58$. As the value of P increased, there

was an initial slow increase in ζ because of decreasing stability of the interface. When P increased above 0.5, there was a transition in the circulation toward the whole deep region being well mixed by an overturning cell driven by both an unstable (to shear) gravity current and the surface convection. This experimental result shows that the shallow side arm must be less than half the depth of the deep region ($H_S/H_D < 0.5$) if the gravity current is to produce a significant stratification in the deep region.

In Fig. 5 we plot results from the two experiments (shown in Figs. 3, 4) in terms of Eq. 13. All the points are seen to fall on the line $\zeta = 3\eta H_{\mathrm{mean}}/H_{\mathrm{max}}$, where $\eta = 0.41$. In future work, it would be interesting to conduct experiments in geometries with more continuous transitions in depth than that shown in Fig. 1, such as wedges or cones. The result of Eq. 13 is expected to hold whenever there are large shallow and deep regions or several shallow side arms connected to one central deep region. Such changes in the geometry could change dramatically the time scales for establishment of the stratification, and we expect a cone-shaped reservoir would have a much smaller initial flushing time scale (Eq. 1) than a wedge-shaped reservoir.
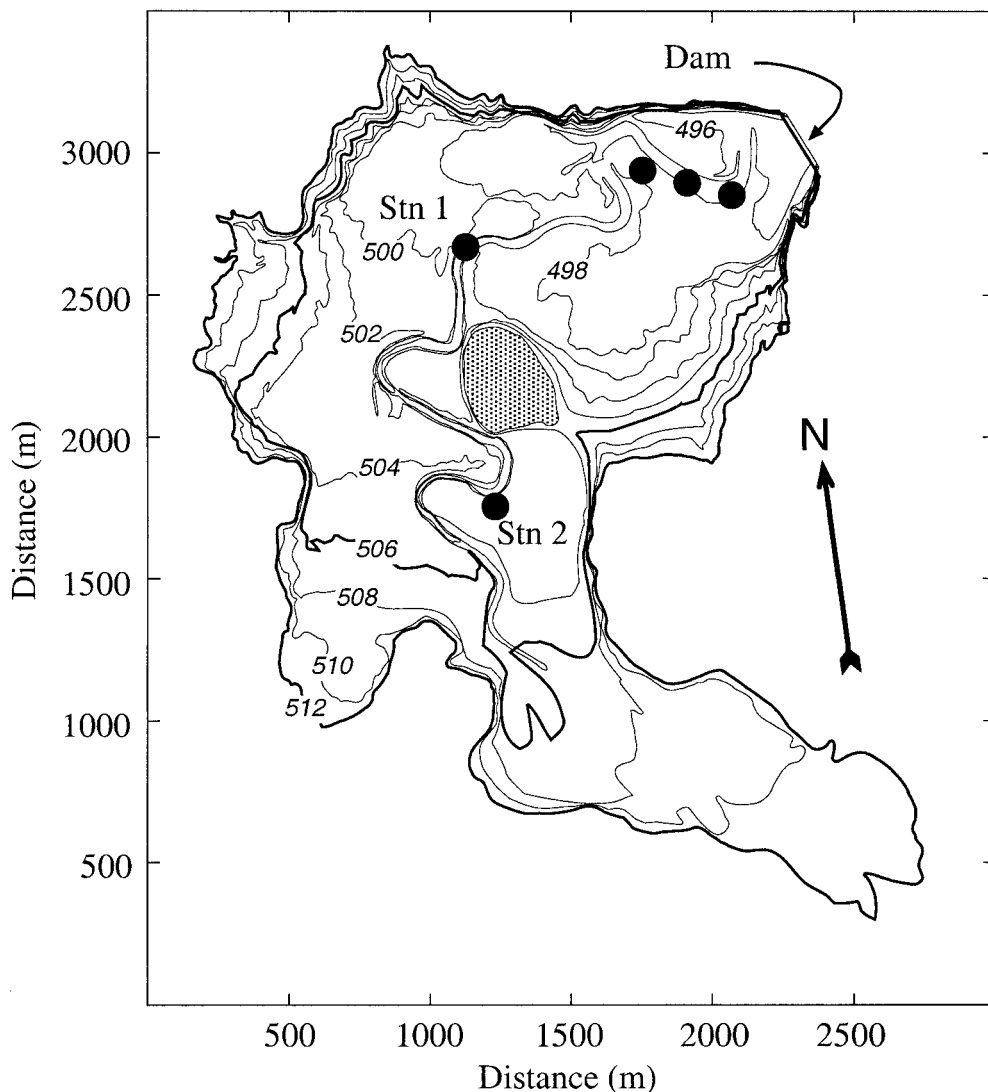
Fig. 6. Bathymetry of Chaffey Reservoir. All levels are meters Australian Height Datum; contours are 2-m intervals. Filled circles denote locations of the weekly CTDO casts. Meteorological station and thermistor chain were located at Stn. 1. Reservoir levels were 506.6 and 512.3 m during the winters of 1995 and 1996, respectively. The drowned river channel is evident along the west side of the island.

Field experiment

Site description and methods—Chaffey Reservoir is located in northeastern New South Wales (31° 21′S, 151°8′E) approximately 32 km southeast of Tamworth at an elevation of 519 m. When full, the reservoir has a capacity of 62,000 ML, a surface area of 542 hectares, a maximum depth of 28 m, and a mean depth of 11.4 m. A drought during 1994–1995 led to a drop in reservoir level to 506 m, equivalent to approximately 20% of capacity, by the beginning of winter (i.e., June 1995). Subsequent inflows increased the level to 512.3 m (~53% capacity) by winter 1996 and to 518.3 m (93% capacity) by winter 1997. The water level was constant to within ±0.1 m throughout each winter.

The reservoir has a deep region extending from roughly the 502-m contour in the south and west to the dam wall at the northeastern corner. To the south, the broad shallow region between the 502- and 506-m contours spans the drowned channel of the Peel River (Fig. 6), the only major source of inflow.

Monitoring of the reservoir took place from February 1995 through November 1997. Meteorological (air temperature, relative humidity, up- and down-welling shortwave and longwave radiation, wind speed, and direction) and thermistor chain data were collected 200 m northeast of Stn. 1 (Fig. 6). The instruments were sampled every 10 s and recorded as 10-min averages from September 1995 to November 1997. Weekly conductivity–temperature–depth-dissolved oxygen (CTDO) profiles with a spatial resolution of 0.25 m were measured in the early morning at 5–6 sites (Fig. 6), depending on water level, using a Seabird Electronics SBE-19 profiler. The sixth site, Stn. 3, was located 3 km
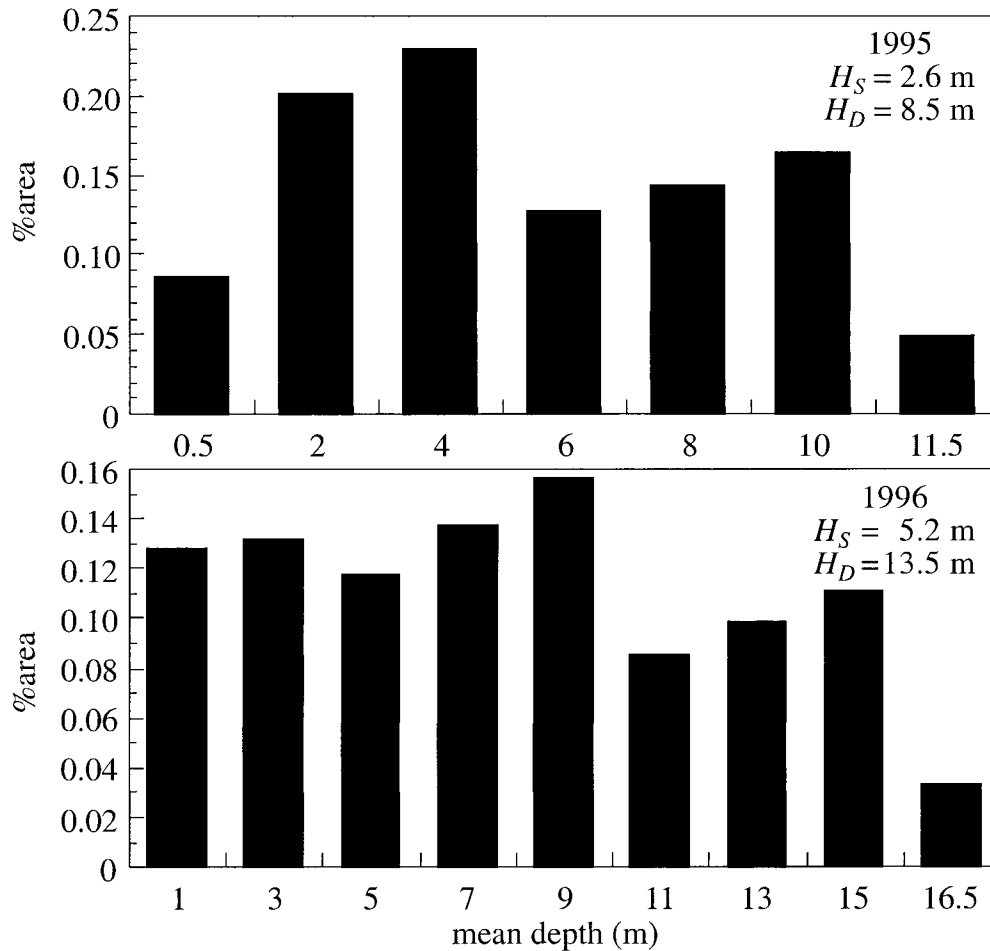
Fig. 7. Depth distributions and areally weighted mean depths of the shallow, H_S, and deep, H_D, regions in Chaffey Reservoir during 1995 and 1996. Peaks in the distribution occur at 4 and 9 m deep in 1995 and 1996, respectively. $R = 0.93$ during 1995 and 0.49 in 1996.

upstream (2.5 km SSE) of Stn. 2 (not shown in Fig. 6) and was only sampled in winter 1997 when the reservoir was nearly full. Full details of the measurement program are given in Sherman et al. (2001).

Calculations: The surface heat flux, $\tilde{H}$, was computed as the sum of the turbulent sensible and latent heat fluxes plus the net emission or absorption of longwave and shortwave radiation. Turbulent heat, mass, and momentum fluxes, adjusted for atmospheric stability, were computed using the air temperature, relative humidity, wind speed, and water surface temperature (0.10 m deep) data following Liu et al. (1979). The velocity scale of the eddies in the convective layer, w^*, was computed using Eq. 16, and observed values of h and $\tilde{H}$ with the buoyancy flux, $B = g\alpha\tilde{H}/\rho C_p$, determined by the surface heat flux $\tilde{H}$.

The expected value of the normalized convective layer depth, ζ_{exp}, was computed from the field data using Eqs. 10 and 13. In Eq. 13, the mean reservoir depth, H_{mean}, was computed as the total volume divided by the total surface area of the reservoir. To determine the maximum depth, H_{max}, the bottom of the reservoir was assumed to be at an elevation

of 497 m, which corresponds to 1% of the reservoir volume when full. Use of Eq. 10 required that R and P be determined from the bathymetry of Chaffey Reservoir (Fig. 6). The boundary between deep and shallow areas was assumed to correspond to the largest peak in the frequency distribution of reservoir depths (Fig. 7). This occurred at roughly the 502-m contour during both years. Areal mean depths, H_S and H_D, were then computed for the shallow and deep regions from the frequency distribution data. The efficiency of the convective deepening process, η, is expected to be within the range 0.36 to 0.43 for the range of Ri_g experienced in the field (Wells et al. 1999).

Results—Meteorology and heat fluxes: During winter 1996 (1 Jun–22 Jul), the average daily net heat flux from the reservoir was −27 W m^{-2}, comprising sensible, latent, and radiative (shortwave + longwave) fluxes of −22, −43, and 38 W m^{-2}, respectively. The mean daily wind speed was 2.2 m s^{-1}. When just the main cooling period is considered (i.e., between 1800 and 0600 h), the corresponding fluxes were −29, −45, and −66 W m^{-2}. Therefore, the typical nighttime cooling flux driving the circulation was −140 W m^{-2} ($B = 3.7 \times 10^{-8}$ m^2 s^{-3}), whereas during the day, there
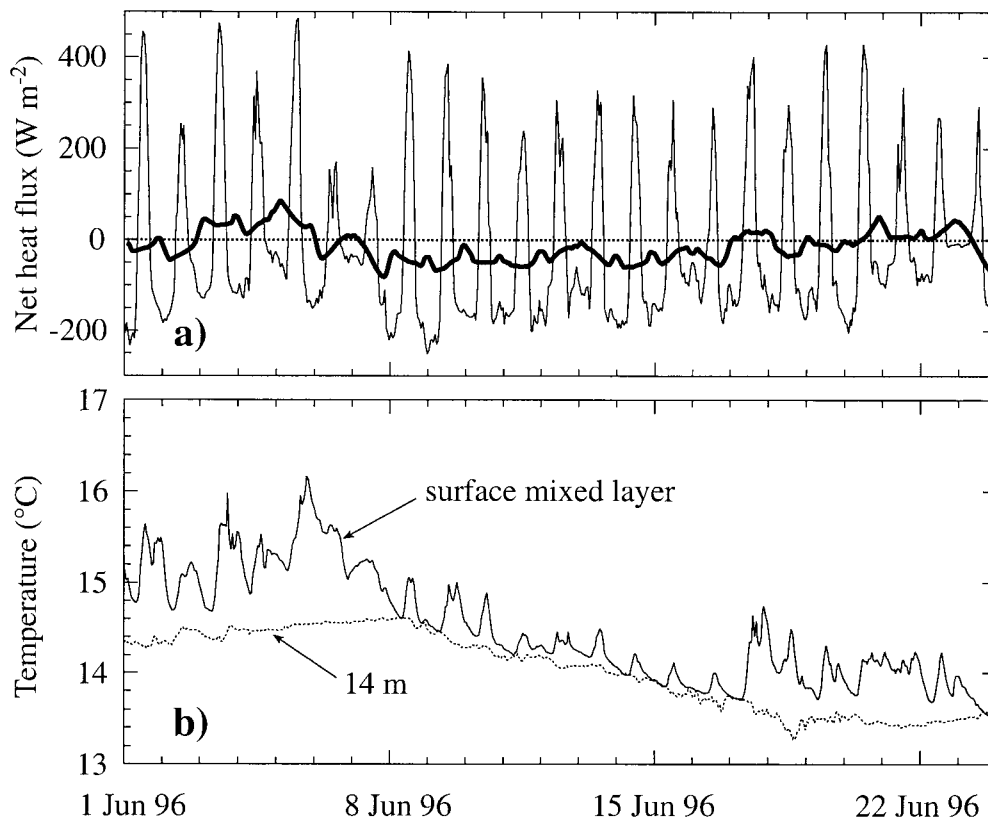
Fig. 8. (a) Net heat flux into Chaffey Reservoir during 1–21 Jun 96. Negative values indicate heat loss from the reservoir. Bold line is the 24-h moving mean. (b) Thermistor chain data from near Sta. 1 showing water temperature in the surface mixed layer and at 14 m deep.

was a net flux of heat into the water. The field experiment is analogous to the laboratory experiments, but with the continuous boundary heat flux replaced by a periodic flux of approximately -140 W m^{-2}.

The periodic nature of the reservoir heat flux is shown in Fig. 8a, and thermistor chain data for the temperatures of the surface mixed layer and at a depth of 14 m are shown in Fig. 8b. The signature of the cold gravity current is particularly noticeable on 9, 12, and 18 Jun 96 when the temperature at 14 m continued to decrease long after the surface layer had started to heat up. Episodes of cooling were of 7–8 d duration and closely corresponded to periods when the 24-h moving mean net heat flux was negative.

Meteorological data were not available for 1995, but 1997 data showed a 10% greater rate of heat loss than occurred in 1996. A 10% change in the heat flux changes the computed time scales (Eqs. 1, 3) by less than 5% and has no effect on the determination of ζ. Therefore, we assumed the same heat flux for both 1995 and 1996 to facilitate comparison of results between years.

Stratification: Temperature profiles at Sta. 1 in Chaffey Reservoir for the winters of 1995 and 1996 are shown in Fig. 9. As each winter progressed, the temperature decreased everywhere throughout the water column while the it remained stratified, with a sharp interface located 4.5–5 m

above the bottom because of the presence of a cold intrusion. At no time during either winter was an isothermal water column observed. The time variation in the surface forcing can be seen in the temperature profile of 20 Jun 95, where a significant cooling event has produced a very cold intrusion in the deep region that is removed by thermal diffusion and subsequent intrusions. The temperature profile shapes are very similar to the equivalent density profiles measured by Wells et al. (1999) in the experiments in which there was a competition between a plume and distributed source in a confined region.

From visual inspection of Fig. 9, we define the convecting layer depth, h, as 6.5 and 12 m during 1995 and 1996, respectively. Profiles measured at the three locations close to the dam wall confirmed the location of the interface at this depth.

It is difficult to determine the interface thickness, Δh, from the field temperature profiles directly, but we can compute its expected range using Eq. 14 and estimating g' and $w*$ from the 1996 field data. During nighttime cooling, $w*$ ranged from 0.005 to 0.013 m s^{-1}. Below the interface, g' was 1.7–5.4×10^{-4} m s^{-2}. Using these values yields $20 < \mathrm{Ri}_g < 160$ and an expected range for Δh of 2.7–3.3 m. Assuming similar $w*$ during 1995 gives $10 < \mathrm{Ri}_g < 80$ and $1.5 < \Delta h < 3.3$.

Normalized convective layer depth and circulation time scales: Using the field data, we can compute the expected
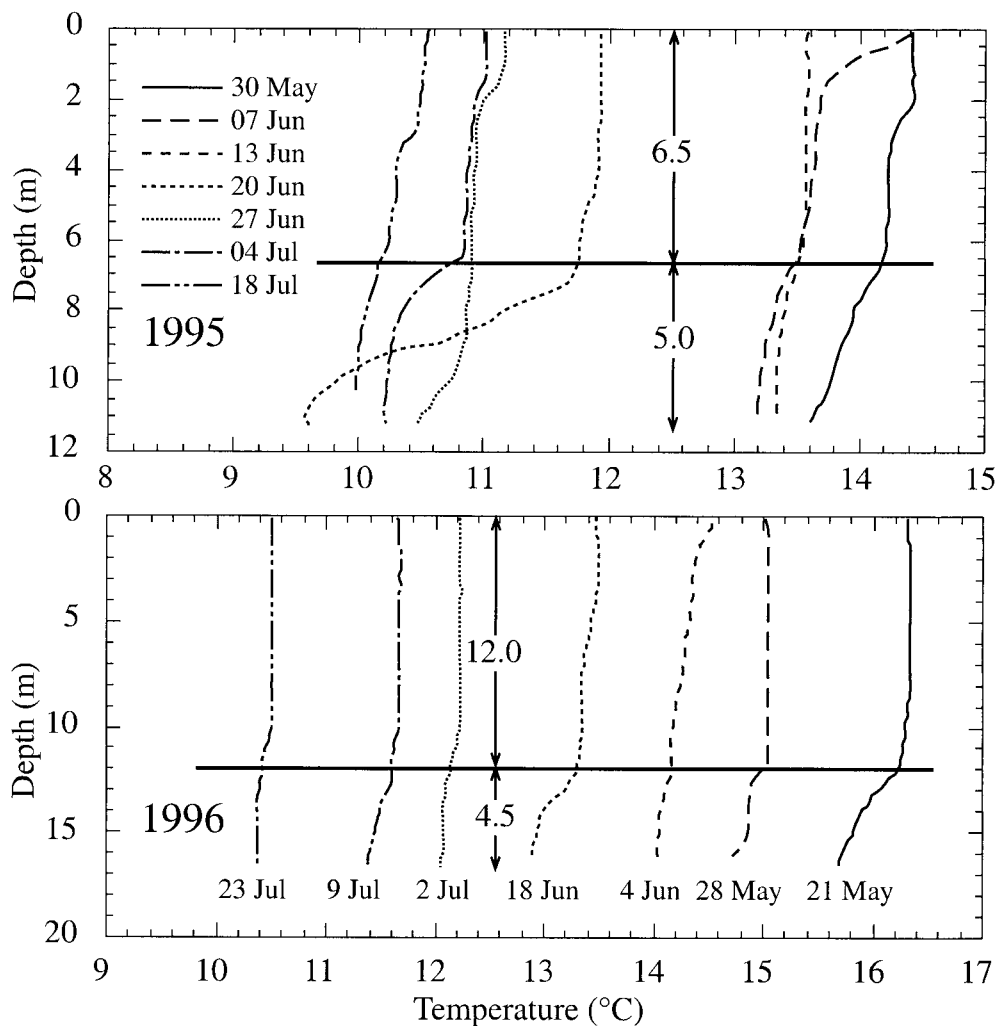
Fig. 9.   Temperature profiles from CTDO casts taken at Sta. 1 during the winters of 1995 (top) and 1996 (bottom). Horizontal rule indicates the boundary between the convecting region near the surface and the stratified region near the bottom caused by the intrusion of cold water. Arrows indicate the thicknesses of the two regions.

normalized convective layer depth, ζ_{exp}, using Eq. 10 and the time scales for the initial setup of the circulation, $\tau_{initial}$, and for the filling of the deep region, τ_{flush}, from Eqs. 1 and 3.

During winter 1995, the surface level was 506.6 m, the areal mean depths of shallow and deep regions, H_S and H_D, were 2.6 m and 8.5 m, respectively, and the shallow region accounted for 52% of the reservoir's surface area. This gives $R = 0.93$ and $P = 0.31$, and we therefore expect a convective layer depth (Eq. 10) of $\zeta_{exp} = 0.71$–0.83 for the likely range of η. The observed convective region thickness was 6.5 m, giving $\zeta_{obs} = 0.76$. We approximated $L_S = 1,500$ m and $L_D = 1,500$ m, and the time scales for the initial establishment of circulation and flushing of the deep region were $\tau_{initial} = 15.9$ h and $\tau_{flush} = 7.6$ d, consistent with the observations of Sherman et al. (2001) that the intrusion appeared to be replenished with colder water on a weekly basis.

By winter 1996, the reservoir filled to 512.3 m and the shallow region shifted significantly toward the southeast (Fig. 6). We approximated $L_S = 3,000$ m, whereas the deep

length was relatively unchanged at $L_D = 1,500$ m. Areal mean depths for the shallow and deep regions were 5.2 and 13.5 m, respectively. With $R = 0.49$ and $P = 0.38$, we found, theoretically, $\zeta_{exp} = 0.63$–0.70. The observed convective layer thickness was 12 m, giving $\zeta_{obs} = 0.86$. The circulation and flushing time scales were $\tau_{initial} = 25.3$ h and $\tau_{flush} = 4.6$ d.

A summary of these results is included in Table 2, which also shows the results of the alternative calculation of ζ using Eq. 13. Compared to Eq. 10, Eq. 13 predicted slightly smaller values of ζ. Note that its use is sensitive to the assumed elevation of the bottom of the reservoir. Had we assumed a bottom elevation of 498 m (1.8% of reservoir volume) rather than 497 m, the two equations would produce virtually identical results.

Discussion

Agreement between the field data, theory, and the laboratory model is good for 1995 but poor for 1996. We believe

Table 2. Summary of field observations and theoretical predictions.

Year	1995	1996
Deep region contour	502 m	502 m
Shallow region contour	506 m	512.3 m
h	6.5 m	12.0 m
L_S	1,500 m	3,000 m
L_D	1,500 m	1,500 m
H_D, areal mean	8.5 m	13.5 m
H_S, areal mean	2.6 m	5.2 m
$P = H_S/H_D$	0.31	0.38
A_D	48% (124 ha)	33% (129 ha)
A_S	52% (132 ha)	67% (265 ha)
V	12,598 ML	32,569 ML
H_{mean}	5.2	8.3
H_{max} (1% volume)	9.0	15.3
$R = A_D/A_S$	0.93	0.49
B	3.7×10^{-8} m^2 s^{-3}	3.7×10^{-8} m^2 s^{-3}
Ri_g	10–80	20–160
η	0.43–0.37	0.40–0.36
Measured ζ	0.76	0.86
Predicted ζ (Eq. 10)	0.71–0.83	0.63–0.70
Predicted ζ (Eq. 13)	0.64–0.75	0.59–0.65
Δh (Eq. 14)	1.2–2.5 m	2.7–3.3 m
$\tau_{initial}$ (Eq. 1)	15.4 h	24.4 h
τ_{flush} (Eq. 3)	7.4 d	4.7 d

the reason for the discrepancy relates to the way in which changes in the geometry in the field interact with the time scales for the forcing and establishment of the convectively driven circulation.

Of particular significance is the periodic forcing in the field, which varies from destabilizing to stabilizing buoyancy fluxes, not only diurnally but also on weekly scales associated with the movement of high and low pressure systems (Fig. 8a). We refer to the time scale of this variation as $\tau_{atmosphere}$ and its value is approximately 12 h. If $\tau_{atmosphere} > \tau_{flush}$, we expect to see a steady, normalized, mixed layer of depth ζ as in the laboratory. If $\tau_{initial} < \tau_{atmosphere} < \tau_{flush}$, we expect to see a gravity current starting to stratify the deep region, but probably with a deeper normalized mixed-layer depth than the predicted ζ because steady state has not yet been reached. If $\tau_{initial} > \tau_{atmosphere}$, then the whole deep region would be well mixed, and although there may be horizontal density differences between deep and shallow regions, no significant gravity current would have time to form.

During 1995, $\tau_{initial}$ was about 16 h (i.e., similar to $\tau_{atmosphere}$), so the circulation in the shallow region had time to become established. In 1996, the shallow region was roughly twice as long ($\tau_{initial} = 25$ h) as in 1995, so the buoyancy flux was never applied long enough for the circulation to become fully established. This means that in 1996 ζ may not have reached the equilibrium described by Eq. 10 and is probably only the consequence of cold water of the shallow region flowing into the deep region after surface cooling had stopped.

Another factor that may contribute to a deeper than expected ζ in the field is the presence of a wind-generated shear stress at the water surface. At Chaffey Reservoir, shear stress

contributes about an additional 20% to the energy available to deepen the surface mixed layer during the winter. This amount is less than 15% of the energy required to explain the additional entrainment observed in the field. The insufficient duration of forcing, therefore, must be a far more significant contributor to the discrepancy in ζ than is wind mixing.

Conclusion—Stratification can occur in reservoirs during periods of winter cooling if the bathymetry can be characterized by distinct deep and shallow regions. If the ratio of the deep areas to the shallow areas of the lake is less than 1 and the ratio of the shallow depth to deep depth is less than 0.5, then a mixed surface layer and a deep stratified region can develop. These reservoirs might otherwise be expected to be well mixed because of convective overturning. Should the cooling persist on a time scale of at least one deep region filling, τ_{flush} (Eq. 3), then theory predicts that a steady state can exist in which the depth of the convecting layer normalized by the depth of the deep region, $\zeta = h/H_D$, is given by $\zeta = 3\eta H_{mean}/H_{max}$, where H_{mean} is the mean reservoir depth, H_{max} is the maximum reservoir depth, and η is a mixing efficiency, typically about 0.4. Laboratory experiments confirmed the functional relationship. In the field H_{max} is sensitive to the level defined (somewhat arbitrarily) as the bottom of the reservoir. To accommodate systems with more complicated geometries, $(R + P)/(1 + R)$ may be substituted for H_{mean}/H_{max}, where R is the ratio of deep and shallow areas and P is the ratio of the mean depths of the deep and shallow regions.

In the field at Chaffey Reservoir, agreement between field data and theory is good for 1995 but poor for 1996. The probable reason for this is that the time scale for the circulation to become fully established, which depends on the length of the shallow region, was close to the time scale of the forcing buoyancy flux during 1995 but much longer in 1996, when the shallow region extended much farther.

The time scales for establishing the circulation in the shallow region and flushing the deep, stratified region suggest that with a typical periodic destabilizing heat flux of -140 W m^{-2}, only reservoirs up to 2–3 km in length will be able to reach the steady circulation observed in the laboratory experiments. Larger reservoirs will still experience convective circulation and, possibly, persistent winter stratification, but the theoretical predictions of the normalized convective layer depth presented here will not be applicable.

An interesting consequence of convectively driven circulation is the significant upward advective transport in the deep region driven by the gravity current. Sherman et al. (2001) concluded that differential cooling was the second strongest vertical transport mechanism in Chaffey Reservoir, behind only the circulation resulting from artificial destratification (by bubble plume injection), and from 2 to 20 times stronger than turbulent diffusion. They proposed also that the associated stratification likely was responsible for the frequent winter blooms of dinoflagellates and buoyant cyanobacteria that are more often associated with strongly stratified water columns during summer and autumn.

Finally, it is important to recognize that convective circulation occurs throughout the year—it is just easier to de-

tect during winter because the gravity current appears as a prominent intrusion along the bottom of the reservoir. At other times of year, the intrusion will insert itself within the water column at its level of neutral buoyancy. The implication is that convective circulation causes significant lateral and vertical transport at all times of the year in water bodies with suitable morphometry.

We envisage that the scaling in this paper should allow a simple prediction of when one might expect to see the formation of winter stratification in a reservoir based on measurements of the bathymetry and heat flux.

References

ADRIAN, R. J., R. T. D. S. FERREIRA, AND T. BOBERG. 1986. Turbulent thermal convection in wide horizontal fluid layers. Exp. Fluids **4:** 121–141.

ARMI, L. 1986. The hydraulics of two flowing layers of different densities J. Fluid. Mech. **163:** 27–58.

ARNOLD, T. N., AND C. E. OLDHAM. 1997. Trace-element contamination of a shallow wetland in Western Australia. Mar. Freshw. Res. **48:** 531–539.

BAINES, W. D., AND J. S. TURNER. 1969. Turbulent buoyant convection from a source in a confined region. J. Fluid. Mech. **37:** 51–80.

DEARDORF, J. W., G. E. WILLIS, AND B. H. STOCKTON. 1980. Laboratory studies of the entrainment zone of a convectively mixed layer. J. Fluid. Mech. **100:** 41–64.

FER, I., U. LEMMIN, AND S. A. THORPE. 2000. The winter cold slope boundary layer, p. 301–305. *In* G. A. Lawrence, R. Pieters, and N. Yonemitsu [eds.], Proceedings of the Fifth International Symposium on Stratified Flows, University of British Columbia, Vancouver, Canada.

FINNIGAN, T. D., AND G. N. IVEY. 1999. Sub-maximal exchange between a convectively forced basin and a large reservoir J. Fluid Mech. **378:** 357–378.

———, and ———. 2000. Convectively driven exchange flow in a stratified sill-enclosed basin. J. Fluid Mech. **418:** 313–338.

GRIMM, T., AND T. MAXWORTHY. 1999. Buoyancy-driven mean flow in a long channel with a hydraulically constrained exit condition. J. Fluid Mech. **398:** 155–180.

HORSCH, G. M., AND H. G. STEFAN. 1988. Convective circulation in littoral water due to surface cooling. Limnol. Oceanogr. **33:** 1068–1083.

JAMES, W. F., AND J. W. BARKO. 1991. Estimation of phosphorus exchange between littoral and pelagic zones during nighttime convective circulation. Limnol. Oceanogr. **36:** 179–187.

LIU, W. T., K. B. KATSAROS, AND J. A. BUSINGER. 1979. Bulk parameterization of the air–sea exchange of heat and water vapor including the molecular constraints at the interface. J. Atmos. Sci. **36:** 1722–1735.

MANINS, P. C., AND J. S. TURNER. 1997. The relation between the flux ratio and energy ratio in a convectively mixed layer. Q. J. R. Met. Soc. **104:** 39–44.

MAXWORTHY, T. 1997. A frictionally and hydraulically constrained model of the convectively driven mean flow in partially enclosed seas. Deep Sea Res. **44:** 1339–1354.

MONISMITH, S. G., J. IMBERGER, AND M. L. MORISON. 1990. Convective motions in the sidearm of a small reservoir. Limnol. Oceanogr. **35:** 1676–1702.

SHERMAN, B. S., AND OTHERS. 2001. The Chaffey Dam story. Final report for Cooperative Research Centre for Freshwater Ecology projects B.202 and B.203. Canberra, May 2001.

STURMAN, J. J., AND G. N. IVEY. 1998. Unsteady convective exchange flows in cavities. J. Fluid Mech. **368:** 127–153.

———, C. E. OLDHAM, AND G. N. IVEY. 1999. Steady convective exchange flows down slopes. Aquat. Sci. **61:** 1–19.

———. 1998. Stratification and circulation produced by heating and evaporation on a shelf. J. Mar. Res. **56:** 1–20.

WELLS, M. G., R. W. GRIFFITHS, AND J. S. TURNER. 1999. Competition between distributed and localized buoyancy fluxes in a confined region. J. Fluid. Mech. **391:** 319–336.